

# Fluorescence dynamics and rate equation analysis in $\text{Er}^{3+}$ and $\text{Yb}^{3+}$ doped double tungstates

Stefan Bjurshagen, Jonas E. Hellström, Valdas Pasiskevicius, Maria Cinta Pujol, Magdalena Aguiló, and Francesc Díaz

The fluorescence dynamics in  $\text{Er}^{3+}$  and  $\text{Yb}^{3+}$  doped  $\text{KGd}(\text{WO}_4)_2$  and  $\text{KY}(\text{WO}_4)_2$  has been investigated. Lifetimes have been measured for the  $\text{Yb}$  ( $^2F_{5/2}$ ),  $\text{Er}$  ( $^4I_{13/2}$ ), and  $\text{Er}$  ( $^4S_{3/2}$ ) levels around 1, 1.5, and 0.55  $\mu\text{m}$ , respectively. The  $\text{Yb}$  ( $^2F_{5/2}$ ) lifetimes show a decreasing trend toward the limiting  $\text{Er}$  ( $^4I_{11/2}$ ) lifetime with increasing  $\text{Er}$ -to- $\text{Yb}$  concentration ratio, whereas the  $\text{Er}$  ( $^4I_{13/2}$ ) lifetimes are mostly unaffected by the doping concentrations. A rate equation analysis has been performed to explain the observed behavior and gain is calculated for a continuous-wave laser at 1.53  $\mu\text{m}$  to find the optimum doping concentrations for high gain. © 2006 Optical Society of America

OCIS codes: 160.3380, 190.7220, 260.2160.

## 1. Introduction

Erbium-doped solid-state lasers are widely used for generation of light in the eye-safe region around 1.5  $\mu\text{m}$ . There are many applications including range finding, remote sensing, optical fiber communication, medicine, and meteorology. As erbium-doped crystals have rather poor absorption at pump-diode wavelengths around 980 nm, the laser efficiency is reduced. For this reason, sensitizer ions such as ytterbium are added to the material to increase the pump absorption and, by means of excitation transfer to erbium ions, improve the laser performance. So far, the  $\text{Er}$ - $\text{Yb}$ -doped phosphate glass<sup>1-3</sup> has been the most efficient laser host in the 1.53  $\mu\text{m}$  wavelength region with the optimum doping concentrations rather well established. Naturally, this material can serve as a benchmark for laser performance in this important spectral range. Other materials that have shown efficient laser operation recently are  $\text{GdCa}_4\text{O}(\text{BO}_3)_3$  ( $\text{GdCOB}$ )<sup>4,5</sup> and  $\text{YCa}_4\text{O}(\text{BO}_3)_3$  ( $\text{YCOB}$ )<sup>6</sup>. However, both phosphate glasses,  $\text{GdCOB}$  and  $\text{YCOB}$ , are far

from perfect laser materials. The main limitations are low thermal conductivity, low threshold for thermal stress-induced fracture as well as relatively low absorption and stimulated-emission cross sections for the  $\text{Yb}^{3+}$  and  $\text{Er}^{3+}$  ions, respectively. For comparison,  $\text{Er}$ - $\text{Yb}$ -doped double-tungstate crystals such as  $\text{KGd}(\text{WO}_4)_2$  ( $\text{KGW}$ )<sup>7</sup> and  $\text{KY}(\text{WO}_4)_2$  ( $\text{KYW}$ )<sup>8,9</sup> offer definite advantages with respect to all these parameters, particularly considering that the  $\text{Yb}^{3+}$  absorption cross section is an order of magnitude larger and that the  $\text{Er}^{3+}$  emission cross section is approximately twice as large in double tungstates than in phosphate glass,  $\text{GdCOB}$ , or  $\text{YCOB}$ . On the other hand, the spectroscopic properties and the dynamics in the  $\text{Er}^{3+}$  and  $\text{Yb}^{3+}$  system are substantially different in double-tungstate crystals. This means that the optimum doping concentrations and proportions, which are critical for efficient laser action, are substantially different in double-tungstate crystals from those in glass,  $\text{GdCOB}$ , or  $\text{YCOB}$ .

Laser action around 1530 nm has been demonstrated before in  $\text{Er}:\text{Yb}:\text{KYW}$ ,<sup>8</sup> but the laser slope efficiency was extremely low with only 1% in absorbed power, which compares unfavorably with phosphate glass,<sup>1,2</sup>  $\text{GdCOB}$ ,<sup>4,5</sup> or  $\text{YCOB}$ .<sup>6</sup> Our objective here is to find the optimum doping concentrations in double tungstates for eye-safe laser applications. We achieve this objective by first investigating relevant spectroscopic and dynamic properties of the  $\text{Er}^{3+}$  and  $\text{Yb}^{3+}$  system in double-tungstate hosts. This involves an experimental study of the excitation dynamics in the crystals with a variety of

S. Bjurshagen (sb@laserphysics.kth.se), J. E. Hellström, and V. Pasiskevicius are with the Department of Physics, Royal Institute of Technology KTH, Roslagstullsbacken 21, 106 91 Stockholm, Sweden. M. Cinta Pujol, M. Aguiló, and F. Diaz are with Fisica I Cristal·lografia de Materials (FiCMA), Universitat Rovira I Virgili, Campus Sescelades C/Marcel·li Domingo, S/N, 43007 Tarragona, Spain.

Received 9 November 2005; revised 21 February 2006; accepted 23 February 2006; posted 27 February 2006 (Doc. ID 65895).

0003-6935/06/194715-11\$15.00/0

© 2006 Optical Society of America

Table 1. Unit Cell Parameters of KREW (RE = Gd, Y and Yb)

Host Crystal	<i>a</i> (Å)	<i>b</i> (Å)	<i>c</i> (Å)	$\beta$ (°)	Ref.
KGW	10.652(4)	10.374(6)	7.582(2)	130.80(2)	10
KYW	10.64	10.35	7.54	130.5(2)	11
KYbW	10.590(4)	10.290(6)	7.478(2)	130.70(2)	12

doping concentrations, which will allow deducing relevant dynamic parameters for the theoretical rate equation model. The modeling then allows mapping of the expected fluorescence and gain versus doping concentrations and will be used to predict optimum concentrations. The influence of four different upconversion processes is also included in the analysis. Throughout this study we compare the relevant spectroscopic parameters of the codoped double tungstates with those experimentally determined in phosphate glass and GdCOB.

## 2. Crystal Samples and Fabrication

The rare-earth potassium tungstates KREW (RE = Gd, Y and Yb) crystallize in the monoclinic system with space group *C2/c*. Their unit cell parameters are reported in Table 1.<sup>10–12</sup> Er<sup>3+</sup>-doped and Er<sup>3+</sup> and Yb<sup>3+</sup> codoped KGW, KYW, and KYbW crystals at several dopant concentrations used in this research were grown at Universitat Rovira i Virgili by means of the top-seeded solution growth slow-cooling method as described in Ref. 13. The solution consisted of K<sub>2</sub>W<sub>2</sub>O<sub>7</sub> as the solvent and a solute:solvent = 11.5/88.5 mol. % as the composition. The solutions used, weighing approximately 195–200 g, were prepared in a cylindrical Pt crucible. The temperature axial and

radial gradients in the solution were 0.1 K/mm and the saturation temperatures were in the 1170–1200 K range. The crystals grew by a seed parallel to the **b** crystallographic direction, without inclusions or any macroscopic defects. A cooling interval of 12 K with a cooling rate of 0.1 K/h for the first 2 K and a lower cooling rate of 0.05 K/h for the next 10 K (an average of 0.055 K/h). During the growth, the seed rotates at 60 rpm without pulling. The crystals were removed slowly from the solution and cooled to room temperature at 15 K/h after 8 days of growth. The average growth rate was approximately  $2 \times 10^{-2}$  g/h. Inclusion-free crystals of approximately 5 g and average dimensions of 10.5 mm × 6 mm × 14 mm along the **a**\* × **b** × **c** crystallographic directions were obtained with the described conditions. The Er and Yb concentrations were measured by electron probe microanalysis. The distribution coefficients for Er and Yb were smaller but close to 1 for KGW and KYW, and slightly larger than 1 for erbium doping in KYbW. A distribution coefficient similar to 1 ensures a good doping homogeneity inside the crystal and an efficient growth procedure. Some commercial Yb-doped KGW and KYW crystals were also included in the experiments. Table 2 lists all the crystals used with their doping concentrations and the crystal thickness in the crystallographic **b** direction, which was used as the propagation direction for pump light. To compare excitation dynamics in other hosts, an Er:Yb:phosphate glass sample, an Yb:GdCOB crystal, and an Er:Yb:GdCOB crystal were also studied.

## 3. Physical Background

Figure 1 shows the energy-level diagram for Er:Yb:KGW and Er:Yb:KYW with relevant pro-

Table 2. Crystals Used in the Experiments with Doping Concentrations

Host Crystal	Er Concentration (mol. %)	Yb Concentration (mol. %)	Er Concentration (10 <sup>20</sup> at./cm <sup>3</sup> )	Yb Concentration (10 <sup>20</sup> at./cm <sup>3</sup> )	Thickness (mm)
KGW	1	—	0.5	—	1.2
	3	—	1.5	—	1.4
	5	—	2.5	—	1.3
	—	5	—	3	3.0
	0.5	5	0.24	2.8	1.7
	0.5	2.5	0.24	1.4	1.85
	2.5	7.5	1.2	4.2	2.0
	1.4	2.5	0.67	1.4	1.7
	5	5	2.4	2.8	2.2
	KYW	5	—	—	—
—		5	—	3	3.0
0.5		5	0.24	2.8	1.3
0.5		2.5	0.24	1.4	2.05
1.5		2.5	0.72	1.4	4.9
KYbW	1	—	0.71	59.4	2.9
	3	—	2.3	57.9	2.75
Glass	2.75	22	2.5	20	1.0
GdCOB	—	10	—	4.2	1.3
	2.5	28	1.0	12	1.5

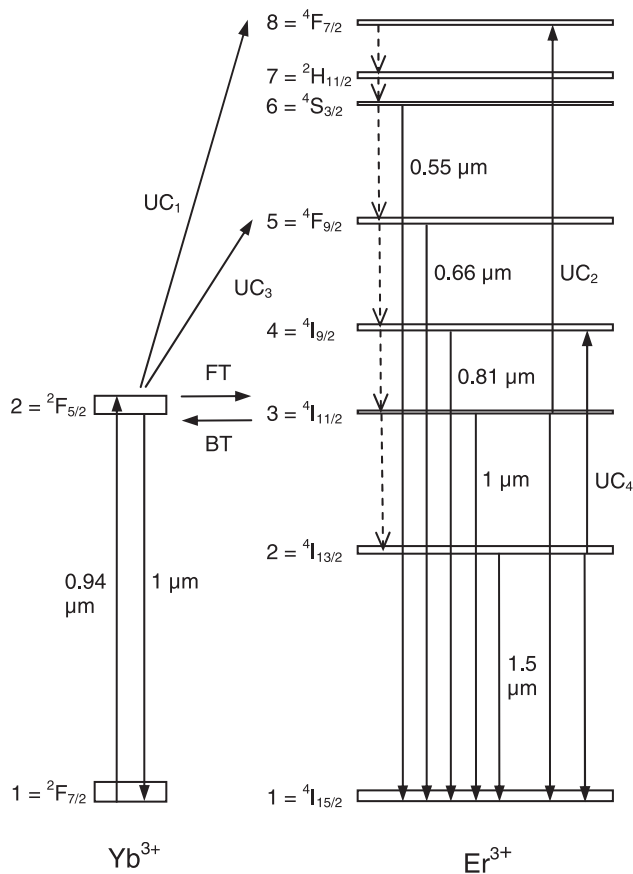


Fig. 1. Energy-level diagram of an Er–Yb double-tungstate system.

cesses, including the pump at  $0.94\ \mu\text{m}$  (in our case), Yb fluorescence around  $1\ \mu\text{m}$ , Er fluorescence around  $1.5\ \mu\text{m}$ , fluorescence at  $0.55$ ,  $0.66$ , and  $0.81\ \mu\text{m}$  resulting from four different upconversion processes ( $\text{UC}_1$ – $\text{UC}_4$ ), and excitation forward transfer (FT) and back transfer (BT) between the Yb and the Er systems. The indexed numbers of Yb ( $i$ ) and Er ( $j$ ) are used according to the labeled energy levels in Fig. 1. During the pumping stage in Yb, corresponding to the  ${}^2F_{7/2} \rightarrow {}^2F_{5/2}$  absorption at  $900$ – $1040\ \text{nm}$ , the population inversion buildup in Er is mainly dependent on the energy forward transfer  $\text{Yb}({}^2F_{5/2}) + \text{Er}({}^4I_{15/2}) \rightarrow \text{Yb}({}^2F_{7/2}) + \text{Er}({}^4I_{11/2})$ , followed by radiative and nonradiative relaxation to the upper laser level  ${}^4I_{13/2}$ . A short nonradiative relaxation lifetime of the  ${}^4I_{11/2}$  level is important, as the nonradiative decay depopulates this level and makes the energy back transfer  $\text{Yb}({}^2F_{7/2}) + \text{Er}({}^4I_{11/2}) \rightarrow \text{Yb}({}^2F_{5/2}) + \text{Er}({}^4I_{15/2})$  less likely. The back transfer process, on the other hand, wastes pump energy that is due to predominantly radiative decay of the Yb ( ${}^2F_{5/2}$ ) level. At the same time, fast depopulation of the  ${}^4I_{11/2}$  level is essential for reducing both the cumulative upconversion ( $\text{UC}_1$ )  $\text{Yb}({}^2F_{5/2}) + \text{Er}({}^4I_{11/2}) \rightarrow \text{Yb}({}^2F_{7/2}) + \text{Er}({}^4F_{7/2})$  and the cooperative upconversion ( $\text{UC}_2$ )  $\text{Er}({}^4I_{11/2}) + \text{Er}({}^4I_{11/2}) \rightarrow \text{Er}({}^4F_{7/2}) + \text{Er}({}^4I_{15/2})$ . These processes divert the excitation from the lasing level,

thus reducing pumping efficiency. Upconverted  $\text{Er}^{3+}$  ions in the  ${}^4F_{7/2}$  level experience a fast nonradiative decay to the  ${}^4S_{3/2}$  manifold. A large part of the upconversion  ${}^4S_{3/2}$  level population relaxes nonradiatively, generating excess heat in the laser crystal. The remainder decays as  ${}^4S_{3/2} \rightarrow {}^4I_{15/2}$  green emission at  $550\ \text{nm}$ . This green fluorescence was clearly observable by the naked eye in all our Er:Yb:KGW and Er:Yb:KYW samples pumped at  $0.94\ \mu\text{m}$ . Two other possible upconversion processes are included in the analysis, as they may decrease the upper laser level  ${}^4I_{13/2}$  directly: cumulative upconversion ( $\text{UC}_3$ )  $\text{Yb}({}^2F_{5/2}) + \text{Er}({}^4I_{13/2}) \rightarrow \text{Yb}({}^2F_{7/2}) + \text{Er}({}^4F_{9/2})$  and cooperative upconversion ( $\text{UC}_4$ )  $\text{Er}({}^4I_{13/2}) + \text{Er}({}^4I_{13/2}) \rightarrow \text{Er}({}^4I_{9/2}) + \text{Er}({}^4I_{15/2})$ .

The nonradiative relaxation of the Er ( ${}^4I_{11/2}$ ) level is determined by the phonon spectrum of the host material, especially high-energy phonon modes that give the fastest nonradiative relaxation in the multiphonon process. For example, the relaxation in phosphate glass is determined by the high-density-of-states phonon mode at  $1200\ \text{cm}^{-1}$ ,<sup>14</sup> in GdCOB the predominant phonon energy is around  $943$  and  $1300\ \text{cm}^{-1}$ ,<sup>15,16</sup> in YCOB the maximum phonon energy available is around  $1550\ \text{cm}^{-1}$ ,<sup>6</sup> whereas the phonons with the frequencies of  $901$  and  $528\ \text{cm}^{-1}$  in KGW,<sup>17</sup>  $530\ \text{cm}^{-1}$  in KYW and  $908$  and  $534\ \text{cm}^{-1}$  modes in KYbW<sup>18</sup> would contribute most. Consequently, phosphate glass, GdCOB, and YCOB should have the fastest nonradiative relaxation, whereas the relaxation in KGW and KYW should be rather slow, leading to the requirement of careful optimization of the doping concentrations in codoped crystals.

#### 4. Measurements of Fluorescence Dynamics

To measure the decay rates of the Er ( ${}^4S_{3/2}$ ) and the Er ( ${}^4I_{11/2}$ ) levels that are predominantly due to multiphonon relaxations, we used singly Er-doped crystals, excited by a frequency-doubled pulsed Nd:YAG laser at  $532\ \text{nm}$ . A beam with a  $3\ \text{ns}$  pulse length and a  $20\ \text{Hz}$  repetition frequency was focused on Er:KGW and Er:KYW crystals at a  $200\ \mu\text{m}$  diameter spot. The fluorescence was collected perpendicular from the excitation direction, passed through an imaging system and appropriate bandpass and pump-rejection filters, and was detected by a Si p-i-n diode. The temporal signal was digitized with a  $5\ \text{Gsample/s}$  sampling rate, by use of a  $1\text{-GHz}$  analog bandwidth oscilloscope. We measured the dynamics of the  $0.55$  and  $1\ \mu\text{m}$  fluorescence for KGW crystals with Er doping concentrations of  $1\%$ ,  $3\%$ , and  $5\%$  and for a  $5\%$  Er-doped KYW crystal. Because of noise in the fluorescence dynamics measurements, an error margin of less than  $5\%$  is estimated for the lifetimes in our system. The result for Er  $1\%$ :KGW is displayed as a semilogarithmic scale in Fig. 2 and the deduced lifetimes of the  ${}^4S_{3/2}$  and  ${}^4I_{11/2}$  levels are  $26$  and  $148\ \mu\text{s}$ , respectively. Table 3 lists a summary of all the results together with values of the  ${}^4I_{11/2}$  lifetime in phosphate glass and GdCOB taken from the literature. Our results are in agreement with measure-

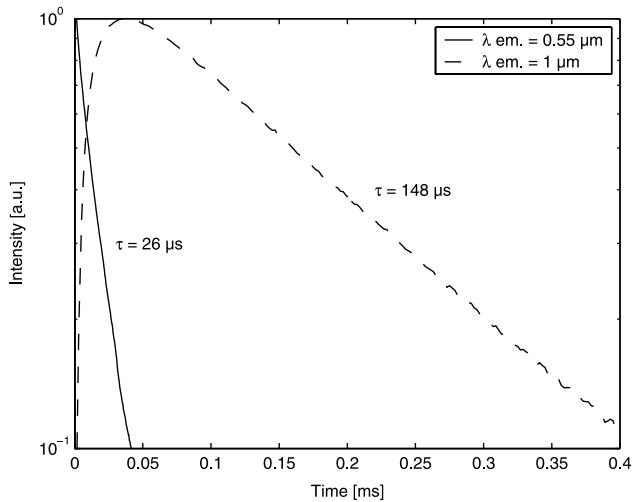


Fig. 2. Dynamics of the emission from the  $^4S_{3/2}$  (solid line) and  $^4I_{11/2}$  (dashed curve) levels in Er 1%:KGW.

ments by Pujol *et al.* (Er:KGW)<sup>19</sup> and Kuleshov *et al.* (Er:KYW).<sup>9</sup> It is evident that the  $^4I_{11/2}$  lifetimes in KGW (151  $\mu\text{s}$  on average) and KYW (123  $\mu\text{s}$ ) are much longer than those in glass (2.5  $\mu\text{s}$ ),<sup>2</sup> GdCOB (0.25  $\mu\text{s}$ ),<sup>4</sup> and YCOB (12.6  $\mu\text{s}$ ).<sup>6</sup> This long lifetime in KGW and KYW will cause significant back transfer and green upconversion in codoped Er–Yb crystals, in contrast to glass, GdCOB, and YCOB, which experience Yb–Er energy transfer followed by rapid relaxation from  $^4I_{11/2}$  to  $^4I_{13/2}$ . Although there is strong upconversion in KGW and KYW, the possibility to realize an upconversion laser is limited, because the lifetime of  $^4S_{3/2}$  is rather short due to the relatively high phonon energy, compared to, e.g., less than  $450\text{ cm}^{-1}$  in Er:LiLuF<sub>4</sub>, leading to a lifetime of 400  $\mu\text{s}$ .<sup>20</sup>

To measure the Er<sup>3+</sup> and Yb<sup>3+</sup> fluorescence dynamics in the codoped samples, which can be used to determine the rates of the energy exchange and relaxation processes, we used an experimental setup employing a nanosecond optical parametric oscillator that generated 3 ns pulses and was tunable between 800 and 1000 nm. The beam was focused in a 200  $\mu\text{m}$  diameter spot and the fluorescence was again col-

lected perpendicular from the excitation direction and was detected by Si and InGaAs p-i-n diodes. The excitation wavelength was tuned to 935 nm where only the Yb<sup>3+</sup> subsystem was excited, thus giving direct access to the resonant energy transfer dynamics. With this detection system, we could observe the fluorescence dynamics of the Yb ( $^2F_{5/2}$ ), Er ( $^4I_{13/2}$ ), and Er ( $^4S_{3/2}$ ) levels. The temporal resolution of the detection system was at least 100 ns, except for low-power green upconversion fluorescence signals, for which a 12  $\mu\text{s}$  resolution was sometimes employed. The resolution was determined by the adjustable resistive–capacitive time constant of the detection system. We could never measure any upconversion fluorescence from the Er ( $^4F_{9/2}$ ) and Er ( $^4I_{9/2}$ ) levels with our detection system, indicating small populations of these levels, which can be due to their fast multiphonon relaxation times (in KYW the relaxation times are 2 and 1  $\mu\text{s}$ , respectively<sup>9</sup>) and that the upconversion mechanisms (UC<sub>3</sub> and UC<sub>4</sub>) that populate these levels directly are relatively weak. The maximum density of the excited Yb<sup>3+</sup> ions constituted only approximately 5% of the Yb<sup>3+</sup> concentration in the KGW and KYW crystals and at these excitation levels we can largely neglect absorption saturation and stimulated emission. The results of the measured rise times and lifetimes are listed in Table 4 and are discussed below.

First, we measured the dynamics of Yb<sup>3+</sup> in Yb:KGW and Er:Yb:KGW. It has been shown that the Yb fluorescence is almost concentration independent in Yb:KYW.<sup>21</sup> Because of the presence of radiation trapping<sup>22,23</sup> for this quasi-three-level transition around 1  $\mu\text{m}$  the relaxation-time measurement results depend on the acceptance angle of the detecting system.<sup>21</sup> Usually, the measured lifetimes are too long because of radiation trapping, but by use of apertures with different pinhole diameters and extrapolation of the lifetime data to zero diameter, efficient elimination of radiation trapping was recently demonstrated in Yb:KYW.<sup>21</sup> A small pinhole reduction of radiation trapping was seen when we measured Yb lifetimes with different detectors: the measured relaxation time with an 0.8 mm<sup>2</sup> area detector was from 6% to 21% smaller than with a 13 mm<sup>2</sup> detector, with the smallest difference observed for samples with a shorter relaxation time. Consequently, we used the small-area detector for dynamics measurements. Also, the fluorescence was selected as close as possible to the crystal side surface and imaged onto the detector to limit the influence of radiation trapping. In Fig. 3 the fluorescence dynamics of the Yb ( $^2F_{5/2}$ ) level in Yb:KGW and some different Er:Yb:KGW crystals is shown on a semilogarithmic scale. The measured relaxation times show a decreasing trend from 438 to 170  $\mu\text{s}$ , and we can clearly see that this trend is coupled to the increased Er-to-Yb concentration ratio in the samples. The relaxation of the Yb<sup>3+</sup> fluorescence in all investigated crystals is determined by the resonant energy transfer, back transfer, and relaxation rate of the Er ( $^4I_{11/2}$ ) level. A

Table 3. Lifetimes of the  $^4S_{3/2}$  and  $^4I_{11/2}$  Levels in Singly Er-Doped Crystals

Host Crystal	Er Concentration (mol. %)	$^4S_{3/2}$ Lifetime ( $\mu\text{s}$ )	$^4I_{11/2}$ Lifetime ( $\mu\text{s}$ )
KGW	1	26	148
	3	23	153
	5	19	151
KYW	5	14	123
Glass	0.9		2.5 <sup>a</sup>
GdCOB	2.5		0.25 <sup>b</sup>

<sup>a</sup>Ref. 2.

<sup>b</sup>Ref. 4.

Table 4. Lifetimes and Rise Times of the Yb ( ${}^2F_{5/2}$ ), Er ( ${}^4S_{3/2}$ ), and Er ( ${}^4I_{13/2}$ ) Levels in Er-Yb-Doped Crystals

Host Crystal	Er Concentration (mol. %)	Yb Concentration (mol. %)	Yb ( ${}^2F_{5/2}$ ) Lifetime ( $\mu$ s)	Er ( ${}^4S_{3/2}$ ) Rise Time ( $\mu$ s)	Er ( ${}^4S_{3/2}$ ) Lifetime ( $\mu$ s)	Er ( ${}^4I_{13/2}$ ) Rise Time ( $\mu$ s)	Er ( ${}^4I_{13/2}$ ) Lifetime (ms)
KGW	—	5	438	—	—	—	—
	0.5	5	273	—	126	252	3.3
	0.5	2.5	229	—	101	240	3.3
	2.5	7.5	222	—	95	222	3.8
	1.4	2.5	212	—	92	207	3.2
KYW	5	5	170	4	71	173	3.6
	—	5	440	—	—	—	—
	0.5	5	341	8.5	111	—	—
	0.5	2.5	262	7.5	95	—	—
KYbW	1.5	2.5	177	6	79	170	3.4
	1	—	(~490)	—	(~115)	—	3.2
Glass	3	—	(~410)	—	(~105)	—	3.8
	—	15.5	1200 <sup>a</sup>	—	—	—	—
GdCOB	2.75	22	12	—	—	—	8.5 <sup>a</sup>
	—	10	2300	—	—	—	—
GdCOB	2.5	28	34	—	—	35	1.16

<sup>a</sup>Ref. 2.

Note: the numbers within parentheses are the next estimated numbers from the measurements in the references.

similar trend was obtained in several Er:Yb:KYW crystals with different doping ratios (see Table 4), and this behavior is analyzed in more detail in Section 5. The dynamics of the Yb fluorescence in stoichiometric double-tungstate  $\text{KYb}_{1-x}\text{Er}_x(\text{WO}_4)_2$  (Er:KYbW) was also measured. Because of the high  $\text{Yb}^{3+}$  excitation and strong upconversion in these samples, the decay was nonexponential. Still, a single-exponential fit can be fitted to the measured data in the tail after 0.5 ms. The resulting tail lifetimes are around 490 and 410  $\mu$ s for Er 1%:KYbW and Er 3%:KYbW, respectively. These lifetimes are, as expected, close to the lifetimes of 438 and 440  $\mu$ s in singly doped Yb 5%:KGW and Yb 5%:KYW, respectively, because of the small Er-to-Yb concentration ratio in Er:KYbW.

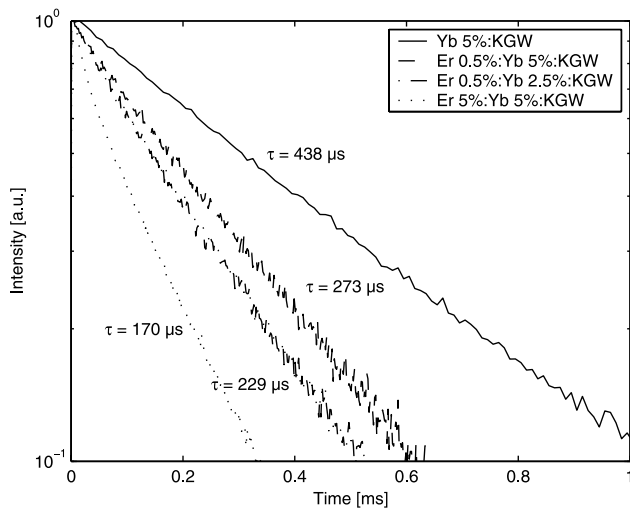


Fig. 3. Fluorescence dynamics from the Yb ( ${}^2F_{5/2}$ ) level around 1  $\mu$ m in Yb:KGW and Er:Yb:KGW.

The green upconversion fluorescence originating from the Er ( ${}^4S_{3/2}$ ) level is much stronger in the co-doped KGW samples than in Er:Yb:GdCOB or Er:Yb:glass. In fact, for the latter materials the upconversion fluorescence was so weak that it was impossible to measure its dynamics with our setup. There are two reasons for strong upconversion in double tungstates: the relatively long lifetime of the Er ( ${}^4I_{11/2}$ ) level and the large efficiency of dipole-dipole interaction between ions, resulting in large coupling constants in the transfer processes. Fast redistribution of the excitation between  $\text{Yb}^{3+}$  and  $\text{Er}^{3+}$  means that the relaxation dynamics of upconversion to a large extent follows that of the long-lived  $\text{Yb}^{3+}$  subsystem. The lifetime increases from around 20  $\mu$ s in singly doped Er:KGW to 126  $\mu$ s in Er 0.5%:Yb 5%:KGW, as seen in Fig. 4. For some samples, we could also measure the short rise times of around 4–8  $\mu$ s.

Finally, all the samples showed substantial fluorescence in the 1.55  $\mu$ m eye-safe spectral region. The fluorescence lifetime measurements (two examples in Fig. 5) showed that the relaxation time constants are mostly unaffected by the doping concentrations in the samples that were available to us. The fluorescence lifetime of approximately 3.2–3.8 ms in Er:Yb:KREW is approximately three times longer than in Er:Yb:GdCOB (1.16 ms) and more than two times shorter than in Er:Yb:phosphate glass (8.5 ms). On the whole, the fluorescence lifetime measurements indicate good potential for the accumulation of excitation energy and thus for an increase in pumping efficiency. We could not see any nonlinear decrease of the Er lifetime in samples with high Er concentration, which indicates that the cooperative upconversion from the Er ( ${}^4I_{11/2}$ ) level ( $\text{UC}_4$ ) is limited. The rise

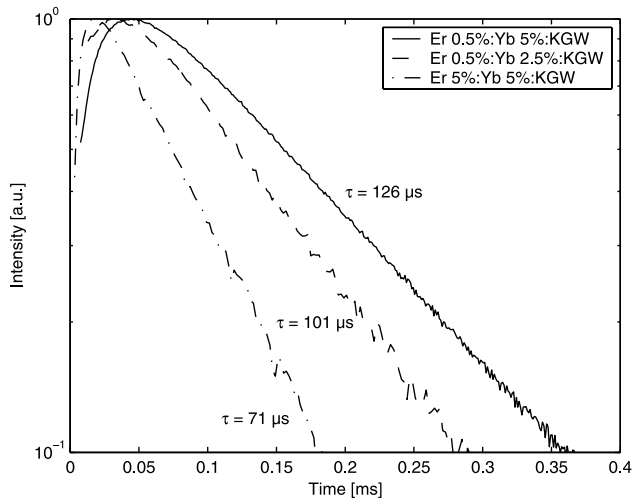


Fig. 4. Dynamics of the green emission from the Er ( $^4S_{3/2}$ ) level at 0.55  $\mu\text{m}$  in Er:Yb:KGW.

time of the fluorescence in the 1.55  $\mu\text{m}$  spectral region originating from the Er ( $^4I_{13/2}$ )  $\rightarrow$  Er ( $^4I_{15/2}$ ) transition is important as it reflects the decay time of the Er ( $^4I_{11/2}$ ) level. The measured rise times are approximately the same as the Yb ( $^2F_{5/2}$ ) lifetimes, and hence the decays of the Yb ( $^2F_{5/2}$ ) and Er ( $^4I_{11/2}$ ) levels are in balance.

### 5. Theoretical Modeling

To model the population levels in Yb and Er and explain the dynamics measured in Section 4, we used a set of rate equations (1)–(6).<sup>24–26</sup> The model includes energy transfer from Yb ( $^2F_{5/2}$ ) to Er ( $^4I_{11/2}$ ), as well as back transfer, upconversion cumulative (UC<sub>1</sub>) and upconversion cooperative (UC<sub>2</sub>) losses to Er ( $^4F_{7/2}$ ), upconversion cumulative (UC<sub>3</sub>) losses to Er ( $^4F_{9/2}$ ), and upconversion cooperative (UC<sub>4</sub>) losses to Er ( $^4I_{9/2}$ ). As the  $^4F_{7/2}$ ,  $^2H_{11/2}$ ,  $^4F_{9/2}$ , and  $^4I_{9/2}$  levels in

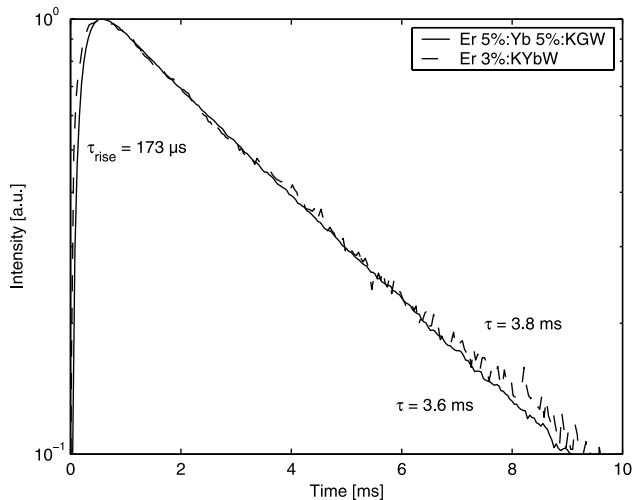


Fig. 5. Dynamics from the Er ( $^4I_{13/2}$ ) level around 1.5  $\mu\text{m}$  in Er 5%:Yb 5%:KGW (solid curve) and in Er 3%:KYbW (dashed curve).

Er shown in Fig. 1 relax rapidly to the next lower-lying level by multiphonon decay, these states have been excluded in the rate equations:

$$\frac{dN_{Yb,2}}{dt} = R_p - \frac{N_{Yb,2}}{\tau_{Yb}} - k_{FT}N_{Er,1}N_{Yb,2} + k_{BT}N_{Yb,1}N_{Er,3} - k_{C,1}N_{Er,3}N_{Yb,2} - k_{C,2}N_{Er,2}N_{Yb,2}, \quad (1)$$

$$\frac{dN_{Er,6}}{dt} = -W_{NR,6}N_{Er,6} - \frac{N_{Er,6}}{\tau_{Er,6}} + k_{C,1}N_{Yb,2}N_{Er,3} + C_{up,1}N_{Er,3}^2, \quad (2)$$

$$\frac{dN_{Er,3}}{dt} = -W_{NR,3}N_{Er,3} - \frac{N_{Er,3}}{\tau_{Er,3}} - k_{BT}N_{Yb,1}N_{Er,3} + k_{FT}N_{Er,1}N_{Yb,2} - k_{C,1}N_{Yb,2}N_{Er,3} - 2C_{up,1}N_{Er,3}^2 + k_{C,2}N_{Yb,2}N_{Er,2} + C_{up,2}N_{Er,2}^2 + W_{NR,6}N_{Er,6} + (\beta_{65} + \beta_{64} + \beta_{63})\frac{N_{Er,6}}{\tau_{Er,6}}, \quad (3)$$

$$\frac{dN_{Er,2}}{dt} = -\frac{N_{Er,2}}{\tau_{Er,2}} - k_{C,2}N_{Yb,2}N_{Er,2} - 2C_{up,2}N_{Er,2}^2 + W_{NR,3}N_{Er,3} + \beta_{32}\frac{N_{Er,3}}{\tau_{Er,3}} + \beta_{62}\frac{N_{Er,6}}{\tau_{Er,6}}, \quad (4)$$

$$N_{Yb} = N_{Yb,1} + N_{Yb,2}, \quad (5)$$

$$N_{Er} = N_{Er,1} + N_{Er,2} + N_{Er,3} + N_{Er,6}. \quad (6)$$

The population densities  $N_{Yb,1-2}$  and  $N_{Er,1-6}$  correspond to the level numbers shown in Fig. 1.  $R_p$  is the pump rate from Yb (1) to Yb (2);  $\tau_{Yb}$ ,  $\tau_{Er,2}$ ,  $\tau_{Er,3}$ , and  $\tau_{Er,6}$  are the radiative lifetimes from the Yb (2), Er (2), Er (3), and Er (6) levels, respectively;  $W_{NR,3}$  and  $W_{NR,6}$  are the nonradiative decay rates from the Er (3) and Er (6) levels, respectively;  $k_{FT}$  is the (forward) energy transfer coefficient,  $k_{BT}$  is the back transfer coefficient,  $k_{C,1}$  is the coefficient of the cumulative upconversion UC<sub>1</sub>,  $C_{up,1}$  is the coefficient of the cooperative upconversion UC<sub>2</sub>,  $k_{C,2}$  is the coefficient of the cumulative upconversion UC<sub>3</sub>,  $C_{up,2}$  is the coefficient of the cooperative upconversion UC<sub>4</sub>,  $\beta_{ij}$  are the branching ratios from the Er ( $i$ ) to the Er ( $j$ ) levels, and  $N_{Yb}$  and  $N_{Er}$  are, respectively, the total Yb<sup>3+</sup> and Er<sup>3+</sup> ion concentrations in the material.

To study the influence of forward transfer and back transfer on the lifetimes of the Yb (2) and Er (3) levels under short-pulse pumping, a system of simplified rate equations that generates single-exponential decays is derived from Eqs. (1) and (3), where low excitation is assumed and therefore upconversion is neglected. At low excitation, the ground-state populations in Er and Yb are left almost unchanged, so that a transfer rate of  $W_{FT} = k_{FT}N_{Er}$  and a back transfer rate of  $W_{BT} = k_{BT}N_{Yb}$  can be used. One could argue that at least the forward transfer coefficient  $k_{FT}$  should be concentration dependent because of the energy migration among Yb ions. Both in glass,<sup>27</sup>

GdCOB,<sup>4</sup> and YCOB,<sup>6</sup>  $k_{FT}$  has been shown to depend on the Yb concentration. However, in Yb:KYW the energy migration is reduced because of the large Yb–Yb distance  $R$ , as the energy transfer between Yb ions scales with  $R^{-6}$ . Because of the slow energy migration, the Yb lifetime is nearly concentration independent in KYW.<sup>21</sup> Because of this evidence of low migration in double tungstates and that the following model agrees well with our experimental results in the range of available doping concentrations, a simplified analysis is made in which the transfer coefficients are assumed concentration independent. Furthermore, the radiative decay from Er (6) and Er (3) is neglected as these levels relax predominantly by nonradiative processes. With these assumptions,  $N_{Yb,2}$  and  $N_{Er,3}$  can be solved from an independent linear system:

$$\frac{dN_{Yb,2}}{dt} = -(W_{Yb} + W_{FT})N_{Yb,2} + W_{BT}N_{Er,3}, \quad (7)$$

$$\frac{dN_{Er,3}}{dt} = W_{FT}N_{Yb,2} - (W_{NR,3} + W_{BT})N_{Er,3}, \quad (8)$$

where  $W_{Yb} = 1/\tau_{Yb}$ . Since the pump pulse is on a nanosecond scale, compared with the other dynamic processes that are on at least a microsecond scale, the initial excitation  $N_{Yb,2}(0)$  is taken as constant. No initial excitation of  $Er^{3+}$  is assumed [ $N_{Er,3}(0) = 0$ ]. The solution to this linear system in Eqs. (7) and (8) is then written as

$$N_{Yb,2}(t) = C_{11} \exp(-W_{eff,1}t) + C_{12} \exp(-W_{eff,2}t), \quad (9)$$

$$N_{Er,3}(t) = C_{21} \exp(-W_{eff,1}t) + C_{22} \exp(-W_{eff,2}t), \quad (10)$$

where the effective rates that determine the population evolutions are

$$W_{eff,1} = \frac{W_{FT} + W_{BT} + W_{Yb} + W_{NR,3}}{2} + \frac{1}{2} [(W_{FT} - W_{BT} + W_{Yb} - W_{NR,3})^2 + 4W_{FT}W_{BT}]^{1/2}, \quad (11)$$

$$W_{eff,2} = \frac{W_{FT} + W_{BT} + W_{Yb} + W_{NR,3}}{2} - \frac{1}{2} [(W_{FT} - W_{BT} + W_{Yb} - W_{NR,3})^2 + 4W_{FT}W_{BT}]^{1/2}, \quad (12)$$

and the constants are given by

$$C_{11} = N_{Yb,2}(0) \frac{W_{FT} + W_{Yb} - W_{eff,2}}{W_{eff,1} - W_{eff,2}}, \quad (13)$$

$$C_{12} = N_{Yb,2}(0) - C_{11}, \quad (14)$$

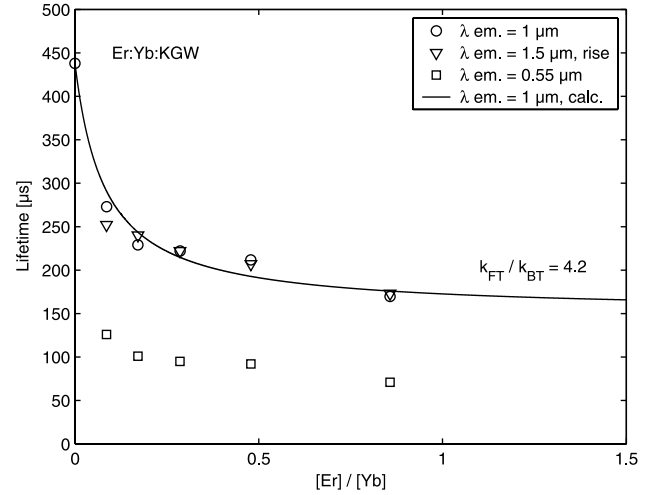


Fig. 6. Measured lifetimes in Er:Yb:KGW versus doping concentration ratio  $[Er]/[Yb]$ : circles, Yb ( ${}^2F_{5/2}$ ) level at  $1 \mu\text{m}$ ; triangles, rise time of the Er ( ${}^4I_{13/2}$ ) level at  $1.5 \mu\text{m}$ ; squares, Er ( ${}^4S_{3/2}$ ) level at  $0.55 \mu\text{m}$ ; solid curve, calculated lifetime of the Yb ( ${}^2F_{5/2}$ ) level with  $k_{FT}/k_{BT} = 4.2$ .

$$C_{21} = C_{11} \frac{W_{FT} + W_{Yb} - W_{eff,1}}{W_{BT}}, \quad (15)$$

$$C_{22} = -C_{21}. \quad (16)$$

$W_{eff,1}$  can be seen as the effective decay (excitation transfer) rate of Yb (2) and effective rise rate of Er (3) at the initial time. At later times, the slower effective decay rate  $W_{eff,2}$  is dominant, which leads to an equal single-exponential decay from Yb (2) and Er (3) according to this model. For our situation with  $W_{Yb}$  and  $W_{NR,3}$  of the same order, a Taylor expansion around  $W_{NR,3} = W_{Yb}$  gives the following approximation of  $W_{eff,2}$  from Eq. (12):

$$W_{eff,2} \approx W_{Yb} + \frac{W_{NR,3} - W_{Yb}}{1 + (W_{FT}/W_{BT})^{-1}}. \quad (17)$$

From approximation (17) we can see that effective lifetime  $1/W_{eff,2}$  depends on  $W_{FT}/W_{BT}$  and thus on the  $[Er]/[Yb]$  concentration ratio. It is further seen that  $W_{eff,2} \rightarrow W_{NR,3}$  when  $W_{FT}/W_{BT} \rightarrow \infty$  and therefore the nonradiative lifetime of the Er ( ${}^4I_{11/2}$ ) level limits the effective lifetime and hence the transfer efficiency that is possible to achieve by optimization of doping concentrations.

Figure 6 displays the Yb ( ${}^2F_{5/2}$ ) fluorescence relaxation time in circles as a function of the  $[Er]/[Yb]$  concentration ratio in different KGW crystals. It shows an initial fast decrease as  $Er^{3+}$  is added to the sample, but then tends to saturation toward the nonradiative lifetime of  $151 \mu\text{s}$  in Er:KGW as the  $Yb^{3+}$  and  $Er^{3+}$  concentrations become approximately equal as predicted by approximation (17). Equation (12) can be fitted by a least-squares approximation to the measured effective lifetimes with a  $k_{FT}/k_{BT}$  constant. The

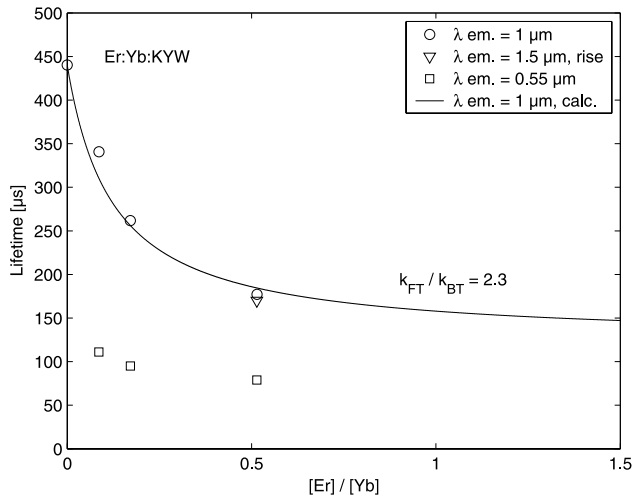


Fig. 7. Measured lifetimes in Er:Yb:KYW versus doping concentration ratio  $[Er]/[Yb]$ : circles, Yb ( $^2F_{5/2}$ ) level at 1  $\mu\text{m}$ ; triangles, rise time of the Er ( $^4I_{13/2}$ ) level at 1.5  $\mu\text{m}$ ; squares, Er ( $^4S_{3/2}$ ) level at 0.55  $\mu\text{m}$ ; solid curve, calculated lifetime of the Yb ( $^2F_{5/2}$ ) level with  $k_{FT}/k_{BT} = 2.3$ .

result is shown as a solid curve for  $k_{FT}/k_{BT} = 4.2$ . This result shows that Eq. (12) and approximation (17) explain the observed behavior in the lifetimes' dependence of doping concentration, at least in the range of doping concentrations available to us. In Fig. 6 the solid curve also corresponds well to the rise time of the Er ( $^4I_{13/2}$ ) level (triangles), which is populated by electrons that relax from the Er ( $^4I_{11/2}$ ) level. The green upconversion decay from Er ( $^4S_{3/2}$ ) is expected to follow  $\exp(-2W_{\text{eff},2}t)$ , as this level is populated by the terms  $k_C N_{Yb,2} N_{Er,3}$  and  $C_{\text{up}} N_{Er,3}^2$  in Eq. (2), where both  $N_{Yb,2}$  and  $N_{Er,3}$  decay as  $\exp(-W_{\text{eff},2}t)$ . In Fig. 6 the green upconversion relaxation time (squares) is actually from 8% to 16% lower than the predicted half-values of the Yb lifetimes. This can be explained by the fact that ions excited by radiation trapping outside the pumped volume can contribute less to upconversion, as the average distance between excited ions increases as the excitation fluency decreases. The same calculations were done for Er:Yb:KYW and are shown in Fig. 7. The results are slightly different as the Er ( $^4I_{11/2}$ ) lifetime is shorter in KYW (123  $\mu\text{s}$ ) and the  $k_{FT}/k_{BT}$  ratio is calculated to 2.3.

It is difficult to distinguish unambiguously which of the two green upconversion processes, the cumulative (UC<sub>1</sub>) or the cooperative (UC<sub>2</sub>), is the most efficient in the codoped samples. Because of the close match in energy differences between the Yb ( $^4F_{5/2}$ )–Yb ( $^4F_{7/2}$ ) and the Er ( $^4I_{11/2}$ )–Er ( $^4F_{7/2}$ ) transitions and the similarities between the cumulative upconversion and the transfer processes, the cumulative upconversion coefficient  $k_{C,1}$  is approximated to be equal to the transfer coefficient  $k_{FT}$  in the following calculations. The influence of the other upconversion processes will be studied below.

Knowing the transfer coefficient  $k_{FT}$  is crucial for proper optimization of the doping concentrations, especially in Er–Yb-doped tungstates in which the life-

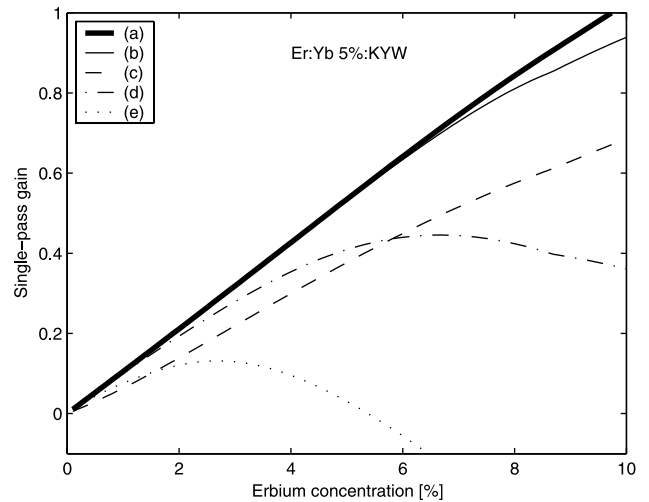


Fig. 8. Calculated single-pass gain including different upconversion processes (UC<sub>1</sub>–UC<sub>4</sub>) in Er:Yb:KYW crystals of 5% Yb concentration and 1 mm thickness at 2 W pump power versus Er concentration. For all curves, (a)–(e)  $k_{C,1} = 5 \times 10^{-15} \text{ cm}^3 \text{ s}^{-1}$ ; thin solid curve, (b)  $C_{\text{up},1} = 5 \times 10^{-15} \text{ cm}^3 \text{ s}^{-1}$ ; dashed curve, (c)  $k_{C,2} = 1 \times 10^{-17} \text{ cm}^3 \text{ s}^{-1}$ ; dash-dot curve, (d)  $C_{\text{up},2} = 1 \times 10^{-18} \text{ cm}^3 \text{ s}^{-1}$ ; dotted curve, (e)  $C_{\text{up},2} = 1 \times 10^{-17} \text{ cm}^3 \text{ s}^{-1}$ .

time of the intermediate Er ( $^4I_{11/2}$ ) level is relatively long. A value of  $k_{FT}$  can be estimated from the measured rise time in the Er ( $^4S_{3/2}$ ) fluorescence. For the sample with the longest rise time of 8.5  $\mu\text{s}$  (Er 0.5%:Yb 5%:KYW), rate equations (1)–(6) were solved numerically for different values of  $k_{FT}$  and in this way a fit of the transfer coefficient to approximately  $(5 \pm 2) \times 10^{-15} \text{ cm}^3 \text{ s}^{-1}$  was achieved. It should be noted that this value is approximately an order of magnitude larger than the value measured in Er:Yb:phosphate glass ( $4.1 \times 10^{-16} \text{ cm}^3 \text{ s}^{-1}$ ) and GdCOB ( $2.9 \times 10^{-16} \text{ cm}^3 \text{ s}^{-1}$ ). This efficient redistribution of the excitation between Yb<sup>3+</sup> and Er<sup>3+</sup> subsystems suggests that the large difference in Er and Yb doping concentrations usually found in glass is not required in KGW and KYW.

As we are interested to find the optimum doping concentrations for laser action in double tungstates, we performed calculations of the gain for the Er ( $^4I_{13/2} \rightarrow ^4I_{15/2}$ ) transition around 1.5  $\mu\text{m}$  in Er:Yb:KYW. The different upconversion processes (UC<sub>1</sub>–UC<sub>4</sub>) are included and their influence is analyzed. For continuous-wave (cw) pumping with a pump rate of  $R_P = W_P(N_{Yb,1} - N_{Yb,2})$ , we solved the rate equations numerically [Eqs. (1)–(6)] at steady state. Here, the pump transition probability is  $W_P = \sigma_P P_P / (h\nu_P \pi w_P^2)$ , where  $\sigma_P$ ,  $P_P$ ,  $h\nu_P$ , and  $w_P$  are the absorption cross section, power, photon energy, and beam radius of the pump, respectively.

Figure 8 shows the single-pass gain  $\sigma(N_{Er,2} - N_{Er,1})l$  at the emission peak versus Er concentration for an Er:Yb:KYW crystal of length  $l = 1 \text{ mm}$ , pumped homogeneously with 2 W in a 100  $\mu\text{m}$  diameter top-hat pump spot at 981 nm. A narrowband pump source such as a Ti:sapphire laser polarized in the  $N_m$  principal optical direction is assumed. In this

direction,  $\sigma_P = 11.7 \times 10^{-20} \text{ cm}^2$  and the maximum stimulated emission cross section is  $\sigma = 2.7 \times 10^{-20} \text{ cm}^2$  at 1534 nm.<sup>28</sup> The Yb concentration is 5% and the thick solid line (a) shows the calculated result, when the green cumulative upconversion (UC<sub>1</sub>) only is included with  $k_{C,1} = 5 \times 10^{-15} \text{ cm}^3 \text{ s}^{-1}$ . This calculation shows the possibility for high gain at this power level with increasing Er concentration. For curves (b)–(e), UC<sub>1</sub> is included and also the influence of an additional upconversion mechanism UC<sub>2</sub>–UC<sub>4</sub> is studied. In thin solid curve (b), strong green cooperative upconversion (UC<sub>2</sub>) is included with  $C_{\text{up},1} = 5 \times 10^{-15} \text{ cm}^3 \text{ s}^{-1}$ , and we can see that the gain is slightly reduced at high Er concentrations.

Because of the weak fluorescence, we have not been able to measure the influence of the other upconversion processes UC<sub>3</sub>–UC<sub>4</sub>, and it is therefore difficult to know the strength of their coefficients  $k_{C,2}$  and  $C_{\text{up},2}$ , respectively. However, we can compare the energy differences of the levels involved in the relevant emissions in Yb<sup>3+</sup> and Er<sup>3+</sup>, respectively, and the relevant excited-state absorptions in Er<sup>3+</sup>, as the microparameters for the upconversion processes strongly depend on the overlap of the emission cross section spectrum of Yb or Er and the excited-state absorption cross section spectrum of Er.<sup>29,30</sup> We compare the results of Er:Yb:KYW with Er:Yb:YCOB used by Burns *et al.*<sup>6</sup> In YCOB, the energy differences of the Er (<sup>4</sup>I<sub>13/2</sub>)–Er (<sup>4</sup>I<sub>15/2</sub>) transition are 6094/6394/6881 cm<sup>-1</sup> (minimum energy difference between Stark levels in upper and lower manifold/zero-to-zero level transition/maximum energy difference between Stark levels in upper and lower manifold) and the energy differences of the Er (<sup>4</sup>I<sub>13/2</sub>)–Er (<sup>4</sup>I<sub>9/2</sub>) transition are 5619/6106/6221 cm<sup>-1</sup>, which indicate a quite good overlap between these transitions, and the cooperative upconversion coefficient in YCOB has been measured to be  $1.30 \times 10^{-17} \text{ cm}^3 \text{ s}^{-1}$ . In KYW,<sup>28</sup> the energy differences of the Er (<sup>4</sup>I<sub>13/2</sub>)–Er (<sup>4</sup>I<sub>15/2</sub>) transition are 6210/6516/6732 cm<sup>-1</sup> and the energy differences of the Er (<sup>4</sup>I<sub>13/2</sub>)–Er (<sup>4</sup>I<sub>9/2</sub>) transition are 5628/5844/6041 cm<sup>-1</sup>, which indicate a much worse overlap between these transitions. For this reason we should expect a lower cooperative upconversion coefficient  $C_{\text{up},2}$  in KYW compared to YCOB. In addition, the energy differences of the Yb (<sup>4</sup>F<sub>5/2</sub>)–Yb (<sup>4</sup>F<sub>7/2</sub>) transition are 9619/10187/10728 cm<sup>-1</sup> and the energy differences of the Er (<sup>4</sup>I<sub>13/2</sub>)–Er (<sup>4</sup>F<sub>9/2</sub>) transition are 8461/8677/8852 cm<sup>-1</sup>, which also indicate a poor overlap between the transitions involved in this cumulative upconversion. We should expect a rather low cumulative upconversion coefficient  $k_{C,2}$  in KYW. With these considerations in mind, we calculated the gain with quite high upconversion coefficients of  $k_{C,2} = 1 \times 10^{-17} \text{ cm}^3 \text{ s}^{-1}$  in Fig. 8(c),  $C_{\text{up},2} = 1 \times 10^{-18} \text{ cm}^3 \text{ s}^{-1}$  in (d), and  $C_{\text{up},2} = 1 \times 10^{-17} \text{ cm}^3 \text{ s}^{-1}$  in (e). It is seen that these processes, especially the cooperative upconversion (UC<sub>4</sub>), significantly reduce the gain. For dotted curve (e), when  $C_{\text{up},2}$  is of the

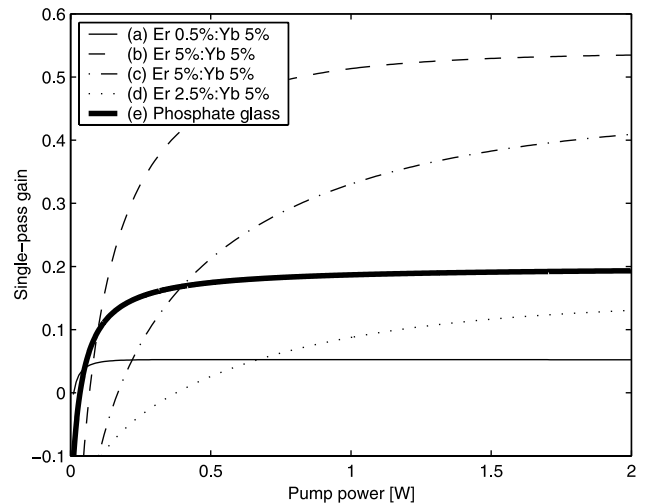


Fig. 9. Calculated single-pass gain in Er:Yb:KYW (a)–(d) and Er 2.75%:Yb 22%:phosphate glass (e) of 1 mm thickness versus pump power. Cumulative upconversion (UC<sub>1</sub>) included in Er:Yb:KYW (a)–(d);  $k_{C,1} = 5 \times 10^{-15} \text{ cm}^3 \text{ s}^{-1}$ . Cooperative upconversion (UC<sub>4</sub>) included in (c)  $C_{\text{up},2} = 1 \times 10^{-18} \text{ cm}^3 \text{ s}^{-1}$  and in (d)  $C_{\text{up},2} = 1 \times 10^{-17} \text{ cm}^3 \text{ s}^{-1}$ .

same order as in YCOB, the optimum Er concentration is 2.7% at this power level of 2 W.

Figure 9 shows the single-pass gain versus pump power for 1 mm long Er:Yb:KYW crystals of different doping concentrations (a)–(d) compared with Er:Yb:phosphate glass with 2.75% Er and 22% Yb (e). Cumulative upconversion (UC<sub>1</sub>) is included in Er:Yb:KYW (a)–(d),  $k_{C,1} = 5 \times 10^{-15} \text{ cm}^3 \text{ s}^{-1}$ . Thin solid line (a) shows the gain of Er 0.5%:Yb 5%:KYW used by Kuleshov *et al.*<sup>8</sup> The gain is rather low, lower than in the Er:Yb:glass sample (e), making the laser sensitive to parasitic losses. For higher Er doping, higher gain is expected as in Er 5%:Yb 5%:KYW (b). Even though the threshold increases, tungstate crystals are more resistant to thermal fracture than phosphate glass, allowing for higher pump powers. Higher gain allows for outcoupling mirrors with higher transmission resulting in suppression of residual losses and higher slope efficiency. Still, because of the long Er (<sup>4</sup>I<sub>11/2</sub>) lifetime, significant green upconversion losses are expected, and the calculated gain is also highly dependent on the possible cooperative upconversion from the upper laser level (UC<sub>4</sub>). In (c), the gain is clearly reduced in this crystal when  $C_{\text{up},2} = 1 \times 10^{-18} \text{ cm}^3 \text{ s}^{-1}$  is assumed. In (d), the coefficient is set to  $C_{\text{up},2} = 1 \times 10^{-17} \text{ cm}^3 \text{ s}^{-1}$  and the Er concentration was chosen to be 2.5% (closer to the optimum concentration in Fig. 8). Here the gain is lower than in the phosphate glass (e), but still higher gain is expected for high powers than for the Er 0.5%:Yb 5%:KYW crystal (a). Our analysis shows the important influence of the upconversion processes in Er–Yb-doped double tungstates. In particular, the influence of the cooperative upconversion from the upper laser level (UC<sub>4</sub>) has to be determined in future work, since the value of  $C_{\text{up},2}$  greatly influences the optimum doping concentrations.

## 6. Conclusions

We have investigated the fluorescence dynamics in Er<sup>3+</sup> and Yb<sup>3+</sup> doped KGW and KYW samples with a variety of doping concentrations. Lifetimes were measured for the Yb (<sup>2</sup>F<sub>5/2</sub>), Er (<sup>4</sup>I<sub>13/2</sub>), and Er (<sup>4</sup>S<sub>3/2</sub>) levels around 1, 1.5, and 0.55 μm, respectively. Because of the relatively long nonradiative lifetime of the Er (<sup>4</sup>I<sub>11/2</sub>) level (around 150 μs in KGW and 120 μs in KYW), strong green Er (<sup>4</sup>S<sub>3/2</sub>) upconversion fluorescence is observed and the Yb (<sup>2</sup>F<sub>5/2</sub>) lifetimes show a decreasing trend toward the limiting Er (<sup>4</sup>I<sub>11/2</sub>) lifetime with increasing Er-to-Yb concentration ratio, whereas the Er (<sup>4</sup>I<sub>13/2</sub>) lifetimes of around 3.5 ms are mostly unaffected by the doping concentrations. A rate equation analysis has been performed to explain the observed behavior, and energy transfer and back transfer coefficients have been estimated. With these results, we calculated gain for an eye-safe cw laser at 1534 nm with KYW crystals of different doping concentrations to find the optimum concentrations for high gain. Our results suggest that higher Er concentrations should be used for high gain than in the previous Er 0.5%:Yb 5%:KYW crystal evaluated in laser experiments,<sup>8</sup> but that the results are greatly influenced by cooperative upconversion from the upper laser level in Er. We intend to determine the value of this coefficient in the future. We have also planned laser experiments with crystals of higher Er concentrations, as predicted by our analysis.

This research has been supported in part by the European Union project under contract NMP3-CT-2003-505580, the Göran Gustafsson Foundation, the Carl Trygger Foundation, and by Comisión Interministerial de Ciencia y Tecnología under projects MAT-2002-04603-C05-03 and MAT-2005-06354-C03.

## References

1. G. Karlsson, V. Pasiskevicius, F. Laurell, J. A. Tellefsen, B. Denker, B. I. Galagan, V. V. Osiko, and S. Sverchkov, "Diode-pumped Er–Yb:glass laser passively Q switched by use of Co<sup>2+</sup>:MgAl<sub>2</sub>O<sub>4</sub> as a saturable absorber," *Appl. Opt.* **39**, 6188–6192 (2000).
2. G. Karlsson, F. Laurell, J. Tellefsen, B. Denker, B. Galagan, V. Osiko, and S. Sverchkov, "Development and characterization of Yb–Er laser glass for high average power laser diode pumping," *Appl. Phys. B* **75**, 41–46 (2002).
3. G. Karlsson, V. Pasiskevicius, F. Laurell, and J. A. Tellefsen, "Q-switching of an Er–Yb:glass microchip laser using an acousto-optical modulator," *Opt. Commun.* **217**, 317–324 (2003).
4. B. Denker, B. Galagan, L. Meva, V. Osiko, S. Sverchkov, I. Voronina, J. E. Hellström, G. Karlsson, and F. Laurell, "Luminescent and laser properties of Yb–Er:GdCa<sub>4</sub>O(BO<sub>3</sub>)<sub>3</sub>: a new crystal for eye-safe 1.5-μm lasers," *Appl. Phys. B* **79**, 577–581 (2004).
5. J. E. Hellström, G. Karlsson, V. Pasiskevicius, F. Laurell, B. Denker, S. Sverchkov, B. Galagan, and L. Meva, "Passive Q-switching at 1.54 μm of an Er–Yb:GdCa<sub>4</sub>O(BO<sub>3</sub>)<sub>3</sub> laser with a CO<sup>2+</sup>:MgAl<sub>2</sub>O<sub>4</sub> saturable absorber," *Appl. Phys. B* **81**, 49–52 (2005).
6. P. A. Burns, J. M. Dawes, P. Dekker, J. A. Piper, H. Jiang, and J. Wang, "Optimization of Er:Yb:YCOB for CW laser operation," *IEEE J. Quantum Electron.* **40**, 1575–1582 (2004).
7. M. Rico, M. C. Pujol, X. Mateos, J. Massons, C. Zaldo, M. Aguiló, and F. Díaz, "Yb sensitising of Er<sup>3+</sup> up-conversion emission in KGd(WO<sub>4</sub>)<sub>2</sub>:Er:Yb single crystals," *J. Alloys Compd.* **323–324**, 362–366 (2001).
8. N. V. Kuleshov, A. A. Lagatsky, V. G. Shcherbitsky, V. P. Mikhailov, E. Heumann, T. Jensen, A. Diening, and G. Huber, "CW laser performance of Yb and Er,Yb doped tungstates," *Appl. Phys. B* **64**, 409–413 (1997).
9. N. V. Kuleshov, A. A. Lagatsky, A. V. Podlipensky, V. P. Mikhailov, A. A. Kornienko, E. B. Dumina, S. Hartung, and G. Huber, "Fluorescence dynamics, excited-state absorption, and stimulated emission of Er<sup>3+</sup> in KY(WO<sub>4</sub>)<sub>2</sub>," *J. Opt. Soc. Am. B* **15**, 1205–1212 (1998).
10. M. C. Pujol, R. Solé, J. Massons, Jna. Gavaldà, X. Solans, C. Zaldo, F. Díaz, and M. Aguiló, "Structural study of monoclinic KGd(WO<sub>4</sub>)<sub>2</sub> and effects of lanthanide substitution," *J. Appl. Cryst.* **34**, 1–6 (2001).
11. S. V. Borisov and R. F. Kletsova, "Crystal structure of KY(WO<sub>4</sub>)<sub>2</sub>," *Sov. Phys. Cryst.* **13**, 517–519 (1968).
12. M. C. Pujol, X. Mateos, M. A. R. Solé, J. Massons, J. Gavaldà, X. Solans, F. Díaz, and M. Aguiló, "Structure, crystal growth and physical anisotropy of KYb(WO<sub>4</sub>)<sub>2</sub>, a new laser matrix," *J. Appl. Cryst.* **35**, 108–112 (2002).
13. R. Solé, V. Nikolov, X. Ruiz, Jna. Gavaldà, X. Solans, M. Aguiló, and F. Díaz, "Growth of β-KGd<sub>1-x</sub>Nd<sub>x</sub>(WO<sub>4</sub>)<sub>2</sub> single crystals in K<sub>2</sub>W<sub>2</sub>O<sub>7</sub> solvents," *J. Cryst. Growth* **169**, 600–603 (1996).
14. C. B. Layne, W. H. Lowdermilk, and M. J. Weber, "Multiphonon relaxation of rare-earth ions in oxide glasses," *Phys. Rev. B* **16**, 10–20 (1977).
15. F. Mougél, G. Aka, A. Kahn-Harari, H. Hubert, J. M. Benitez, and D. Vivien, "Infrared laser performance and self-frequency doubling of Nd<sup>3+</sup>:Ca<sub>4</sub>GdO(BO<sub>3</sub>)<sub>3</sub> (Nd:GdCOB)," *Opt. Mater.* **8**, 161–173 (1997).
16. A. Lupei, G. Aka, E. Antic-Fidancev, B. Viana, D. Vivien, and P. Aschehoug, "Selective excitation study of Yb<sup>3+</sup> in GdCa<sub>4</sub>O(BO<sub>3</sub>)<sub>3</sub> and YCa<sub>4</sub>O(BO<sub>3</sub>)<sub>3</sub>," *J. Phys. Condens. Matter* **14**, 1107–1117 (2002).
17. L. Macalik, J. Hanuza, and A. A. Kaminskii, "Polarized infrared and Raman spectra of KGd(WO<sub>4</sub>)<sub>2</sub> and their interpretation based on normal coordinate analysis," *J. Raman Spectrosc.* **33**, 92–103 (2002).
18. J. Hanuza and L. Macalik, "Polarized infra-red and Raman spectra of monoclinic α-KLn(WO<sub>4</sub>)<sub>2</sub> single crystals (Ln = Sm–Lu, Y)," *Spectrochim. Acta A* **43**, 361–373 (1987).
19. M. C. Pujol, M. Rico, C. Zaldo, R. Solé, V. Nikolov, X. Solans, M. Aguiló, and F. Díaz, "Crystalline structure and optical spectroscopy of Er<sup>3+</sup>-doped KGd(WO<sub>4</sub>)<sub>2</sub> single crystals," *Appl. Phys. B* **68**, 187–197 (1999).
20. E. Heumann, S. Bär, H. Kretschmann, and G. Huber, "Diode-pumped continuous-wave green upconversion lasing of Er<sup>3+</sup>:LiLuF<sub>4</sub> using multipass pumping," *Opt. Lett.* **27**, 1699–1701 (2002).
21. K. Petermann, D. Fagundes-Peters, J. Johannsen, M. Mond, V. Peters, J. J. Romero, S. Kutovoi, J. Speiser, and A. Giesen, "Highly Yb-doped oxides for thin-disc lasers," *J. Cryst. Growth* **275**, 135–140 (2005).
22. D. S. Sumida and T. Y. Fan, "Effect of radiation trapping on fluorescence lifetime and emission cross section measurements in solid-state laser media," *Opt. Lett.* **19**, 1343–1345 (1994).
23. C. D. Marshall, S. A. Payne, L. K. Smith, H. T. Powell, W. F. Krupke, and B. H. T. Chai, "1.047-μm Yb:Sr<sub>5</sub>(PO<sub>4</sub>)<sub>3</sub>F energy storage optical amplifier," *IEEE J. Sel. Top. Quantum Electron.* **1**, 67–77 (1995).
24. L. F. Johnson, H. J. Guggenheim, T. C. Rich, and F. W. Ostermayer, "Infrared-to-visible conversion by rare-earth ions in crystals," *J. Appl. Phys.* **43**, 1125–1137 (1972).
25. J. A. Hutchinson, H. R. Verdun, B. H. T. Chai, B. Zandi, and

- L. D. Merkle, "Spectroscopic evaluation of  $\text{CaYAlO}_4$  doped with trivalent Er, Tm, Yb and Ho for eyesafe laser applications," *Opt. Mater.* **3**, 287–306 (1994).
26. B. Simondi-Teisseire, B. Viana, D. Vivien, and A. M. Lejus, " $\text{Yb}^{3+}$  to  $\text{Er}^{3+}$  energy transfer and rate-equations formalism in the eye safe laser material  $\text{Yb:Er:Ca}_2\text{Al}_2\text{SiO}_7$ ," *Opt. Mater.* **6**, 267–274 (1996).
27. V. P. Gapontsev, S. M. Matitsin, A. A. Isineev, and V. B. Kravchenko, "Erbium glass lasers and their applications," *Opt. Laser Technol.* **14**, 189–196 (1982).
28. X. Mateos, R. Solé, Jna. Gavaldá, M. Aguiló, J. Massons, and F. Díaz, "Crystal growth, optical and spectroscopic characterization of monoclinic  $\text{KY}(\text{WO}_4)_2$  co-doped with  $\text{Er}^{3+}$  and  $\text{Yb}^{3+}$ ," *Opt. Mater.* **28**, 423–431 (2006).
29. J. A. Caird, A. J. Ramponi, and P. R. Staver, "Quantum efficiency and excited-state relaxation dynamics in neodymium-doped phosphate laser glasses," *J. Opt. Soc. Am. B* **8**, 1391–1403 (1991).
30. M. Laroche, S. Girard, J. K. Sahu, W. A. Clarkson, and J. Nilsson, "Accurate efficiency evaluation of energy-transfer processes in phosphosilicate  $\text{Er}^{3+}$ - $\text{Yb}^{3+}$ -codoped fibers," *J. Opt. Soc. Am. B* **23**, 195–202 (2006).